Journal of
Applied Crystallography

ISSN 0021-8898

Received 16 August 2006
Accepted 25 February 2007

© 2007 International Union of Crystallography
Printed in Singapore – all rights reserved

Initial process of amyloid formation of apomyoglobin and effect of glycosphingolipid G_{M1}

Teruaki Onai,[a] Masaharu Koizumi,[a] Han Lu,[a] Katsuaki Inoue[b] and Mitsuhiro Hirai[a]*

[a]Department of Physics, Gunma University, Maebashi 371-8510, Japan, and [b]Japan Synchrotron Radiation Research Institute, Sayo Hyogo 679-5198, Japan. Correspondence e-mail: mhirai@fs.aramaki.gunma-u.ac.jp

Using small-angle and wide-angle X-ray scattering techniques it has been possible to clarify the helix-to-sheet (cross-β) transition and the stacking process of the cross-β sheet of apomyoglobin as a model for amyloid. The present results indicate that the cross-β formation and the pleated sheet stacking start concurrently and that the stacking continues progressively after the saturation of the cross-β formation. The effect of glycosphingolipids on the above processes has also been studied. At high molar ratio of glycosphingolipid to apomyoglobin the growth of the amyloid is suppressed.

1. Introduction

The mechanism by which proteins fold into their native structures poses a rather puzzling problem that has been extensively discussed (Pain, 2000; Oliveberg & Wolynes, 2006). For clarifying the mechanism of protein folding, it is important to observe detailed features of folding–unfolding processes of proteins by using various methods (Dobson, 2004). On the other hand many proteins have been found to be involved in diseases through misfolding, which are called protein-folding diseases such as amyloidosis (Grateau *et al.*, 2004). The factors that might accelerate amyloid formation are diverse, that is, mutation, increase of protein concentration and infection are considered to induce amyloid formation. Amyloid structures of proteins are stable but different from those native structures that are encoded in the amino acid sequences. The proteins forming amyloid deposits both in extra and intra cells possess diverse features in structural classes, sequence patterns and intramolecular interactions. Thus, the formation of amyloid aggregates would not be special for some distinctive proteins but may be ruled by some general physicochemical mechanism. Several globular proteins such as apomyoglobin (ApoMY) and lysozyme have been found to form amyloid fibrils (Dyson & Wright, 2004). The studies of amyloid formation of these proteins under various conditions might possibly clarify an insight on the general mechanism.

Thus the mechanism of amyloid formation has not only physiological and pathological significance but also includes an essential problem in protein folding, namely that a globular folded structure of a native protein is not necessarily a unique stable structure defined by Anfinsen's dogma (Anfinsen, 1973). Therefore it is important to clarify how helix-to-sheet transition occurs to form cross-β structure at an initial stage of amyloid formation and what factor affects or induces such a transition. On one of the candidates effectively inducing amyloid formation, previous spectroscopic studies using fluorescence spectroscopy and circular dichroism (Choo-Smith *et al.*, 1997; Matsuzaki & Horikiri, 1999) showed that amyloid β proteins (Aβ) interact strongly with monosialogangliosides (G_{M1}) to promote a structural transition of Aβ from helix to sheet and that G_{M1}-bound Aβ is suggested to form seeds in the course of Aβ polymerization to amyloid fibril (Hayashi *et al.*, 2004). G_{M1} is one of the species of gangliosides. Gangliosides, major components of glycosphingolipids, are rich in neuronal cells and form lipid microdomains, so-called rafts, with other particular lipids and proteins. The function of rafts is also one of the current hot topics in cell biology since rafts are assumed to have significant functions in signal transduction, cell adhesion and lipid/protein sorting (Hakomori, 2001).

By using a model system of amyloid, we have carried out small-angle X-ray scattering (SAXS) and wide-angle X-ray scattering (WAXS) measurements to elucidate an initial stage of amyloid formation, namely, a helix-to-sheet (cross-β) transition of a protein followed by the amyloid polymerization and to clarify an effect of gangliosides on the above process. Functions of membrane proteins involved in signaling would be affected through accumulation of amyloid proteins. We assume that the complexation of Aβ proteins with gangliosides and the polymerization of Aβ proteins to amyloid fibril change the membrane structure and dynamics to disturb normal signal transduction. In the present experiments we have used ApoMY as a model protein of amyloid deposit because ApoMY has been studied for four decades using SAXS (Kirste *et al.*, 1969) and is known to adopt two well defined different structures: the helix-rich native structure and the cross-β structure at pH 9 and 338 K (Fändrich *et al.*, 2001). By using high-intensity X-rays from a third generation synchrotron source (SR), we demonstrated that the WAXS method has a great advantage in that it allows the direct observation of the whole hierarchical structures of proteins such as quaternary, tertiary, domain and secondary structures in solutions (Hirai *et al.*, 2002). We have recently clarified the detailed aspects of the thermal unfolding and refolding of a globular protein, hen egg-white lysozyme (HEWL) depending on structural hierarchy, where we found that the structural transition cooperativeness among hierarchical structures significantly depends on solvent conditions and on the stability of the domains within the protein (Hirai *et al.*, 2004). Based on our previous results of protein folding using SR-SAXS (Hirai *et al.*, 1998, 1999; Arai & Hirai, 1999) and SR-WAXS, we have studied the detailed features of the transition of ApoMY to amyloid depending on solvent condition and on the presence of gangliosides.

Amyloid fibril formation has been assumed to proceed basically through the following three steps. At the first step, native protein changes its conformation to a β-sheet rich structure, called a cross-β structure, that is dominated by interactions of main chains commonly within different polypeptides. After this conformational transition, the proteins are polymerized and form pleated sheets, and these sheets are stacked to form a proto-filament. Finally, these filaments

assemble with each other and form a higher-ordered fiber, a so-called amyloid fibril. Many studies have been executed intensively by using various techniques (Dobson, 2004). Electron microscopy, atomic force microscopy, fluorescent probe microscopy and X-ray fiber diffraction methods have been employed for studying mainly the third step and the final products. Other techniques such as circular dichroism and FT-infrared spectroscopy have been used for studying the first step. On the other hand, the information on the second step is still less abundant. This step would have a great importance since misfolded or unfolded proteins should form amyloid nuclei and should be polymerized to take a pleated-sheet stacking. X-ray solution scattering has been a great advantage to studying such nano-scaled structures. The use of the high-intensity X-ray from the third generation synchrotron source especially, can be expected to clarify detailed information covering mostly whole steps of amyloid formation.

2. Materials and methods

2.1. Sample preparation

ApoMY and myoglobin (MY) from horse skeletal muscle, monosialoganglioside (G_{M1}) from bovine brain and cholesterol were purchased from SIGMA Chemical Co. (USA) and were used without further purification. All other chemicals used were of analytical grade. The small unilamellar vesicle containing [G_{M1}]/[cholesterol] = 1/1 was prepared by a method given elsewhere (Hirai *et al.*, 2003, 2005). The buffer solvents used were 50 m*M* Tris–HCl (2-amino-2-hydroxymethyl-1,3-propanediol hydrochloride) buffer at pH 7–9 and 50 m*M* sodium acetate buffer at pH 3–5.5. The sample at pH 2 was prepared by dissolution into low pH solvent adjusted with hydrochloric acid. The final pH values of the samples were measured after the dissolution of proteins in buffers. The protein concentration for SAXS and WAXS measurements were from 0.005 g ml^{-1} (2.8 x 10^{-4} mol l^{-1}) to 0.03 g ml^{-1} (1.7 x 10^{-3} mol l^{-1}).

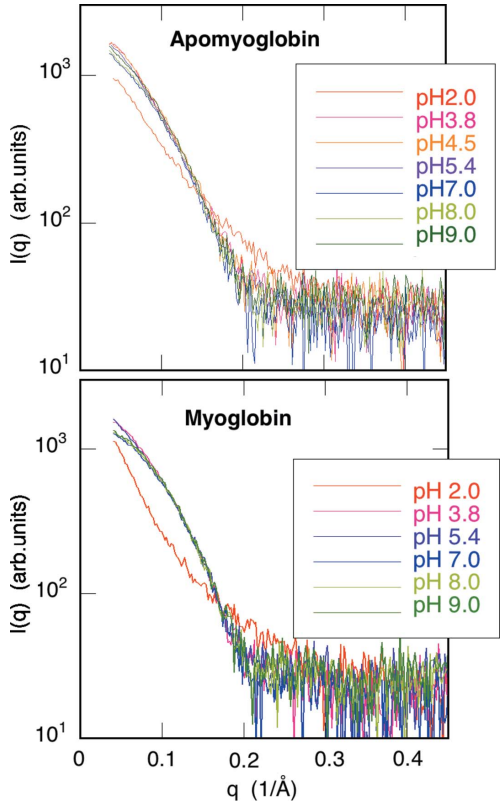

Figure 1
pH dependence of SAXS curves $I(q)$ of ApoMY in comparison with those of MY at 298 K. The protein concentrations are 0.01 g ml^{-1}.

2.2. Small-angle and wide-angle X-ray scattering measurements

SAXS experiments were performed by using the spectrometer installed at BL-10C of the 2.5 GeV synchrotron radiation source (PF) at the High Energy Accelerator Research Organization, Tsukuba, Japan. The X-ray wavelength, the sample-to-detector distance and the exposure time were 1.49 Å, 190 cm and 300 s, respectively. A one-dimensional position-sensitive proportional counter was used. WAXS experiments were performed by using the spectrometer installed at BL-40B2 of the 8 GeV synchrotron radiation source (SPring-8) at the Japan Synchrotron Radiation Research Institute, Harima, Japan. WAXS intensity was recorded on an imaging plate system from Rigaku R-AXIS IV. Details about the spectrometer are described elsewhere (Miura *et al.*, 2000). The X-ray wavelength and the sample-to-detector distance and the exposure time were 0.82 Å (or 1.0 Å), 41 cm and 30 s, respectively. In WAXS measurements the sample solution was moved oscillatory to avoid radiation damage on the sample due to the small beam size (~0.1 mm^2). Other conditions were as given previously (Hirai *et al.*, 1999, 2004). Under the present measurement conditions some radiation damages would be negligible since the observed scattering patterns were fitted well by the theoretical ones based on the crystallographic data as shown previously (Hirai *et al.*, 2002, 2004).

2.3. Scattering data treatment and analysis

The background correction from solvents is quite important for WAXS experiments of diluted protein solutions because scattering intensities above q ~0.8 Å^{-1}, are dominated by scatterings from the solvent and show a broad correlation peak at ~2.0 Å^{-1}. In the background correction of WAXS data the following equation can be used empirically to obtain the net scattering $I(q)$ from the proteins (Hirai *et al.*, 2002, 2004).

$$I_q = [I_{\rm sol}(q)/(B_{\rm sol}T_{\rm sol}) - I_{\rm cell}(q)/(B_{\rm cell}T_{\rm cell})]/P_{\rm sol} - (1 - cv_\alpha)[I_{\rm solv}(q)/(B_{\rm solv}T_{\rm solv}) - I_{\rm cell}(q)/(B_{\rm cell}T_{\rm cell})]/P_{\rm sol}, \quad (1)$$

where $I_{\rm sol}(q)$, $I_{\rm solv}(q)$, $I_{\rm cell}(q)$, $B_{\rm sol}$, $B_{\rm solv}$, $B_{\rm cell}$, $T_{\rm sol}$, $T_{\rm solv}$ and $T_{\rm cell}$ are the observed scattering intensities, the incident beam intensities, and the transmissions of the solution and the solvent at each temperature, and the sample cell, respectively. $P_{\rm sol}$ and $P_{\rm solv}$ are the water-correlation peak intensities of the solution and the solvent; c and v_α are the concentration of the protein molecule and its partial specific volume, respectively. The v_α value used was 0.74 ml g^{-1} for MY (Gekko & Hasegawa, 1986). After the background corrections above, the following standard analyses were carried out by a method reported previously (Hirai *et al.*, 1998, 1999). The distance distribution function $p(r)$ was obtained by Fourier transform of the observed scattering intensity $I(q)$ as

$$p(r) = \frac{1}{2\pi^2}\int_0^\infty rqI(q)\sin(rq)\mathrm{d}q, \quad (2)$$

where $q = (4\pi/\lambda)\sin(\theta/2)$, θ and λ are the scattering angle and the X-ray wavelength. The radius of gyration $R_{\rm g}$ was determined by

$$R_{\rm g}^2 = \frac{\int_0^{D_{\rm max}} p(r)r^2\mathrm{d}r}{2\int_0^{D_{\rm max}} p(r)\mathrm{d}r}, \quad (3)$$

where D_{max} is the maximum diameter of the particle, estimated from the $p(r)$ function satisfying the condition $p(r) = 0$ for $r > D_{max}$.

3. Results and discussion

3.1. Tertiary structure of apomyoglobin depending on pH

Fig. 1 shows a comparison of the pH dependence of SAXS curves $I(q)$ for ApoMY and MY. It can be seen that the curves for ApoMY and MY show minor changes in the pH range from 3.8 to 9.0 under the present solvent conditions. At the lowest pH of 2.0, the $I(q)$ of ApoMY and MY change to show a steep increase of the scattering intensity below q = 0.1 Å^{-1}, suggesting that the tertiary structures of ApoMY and MY change to be expanded ones. Fig. 2 shows the Kratky plots [$q^2I(q)$ *versus* q] of the SAXS curves in Fig. 1. The Kratky plots are known to reflect well the changes of polypeptide chain structures in interactions between polymer elements, local conformations and rigidities within polymer chains (Kirste & Oberthür, 1982). As seen in Fig. 1, the Kratky plots also show little change within the pH range from 3.8 to 9.0, however, at pH 2.0 the Kratky plots change significantly with the loss of the broad peak at q = ~0.1 Å^{-1}, indicating that at pH 2 both proteins lose their compactness in the tertiary structures as reported for acid denatured states (Goto *et al.*, 1990). The Kratky plots above q = ~0.2 Å^{-1} alter from an undulating slope to an asymptotic one, suggesting that the persistency of the polypeptide chain holds locally for both proteins in spite of pH variation which is similar to the case of HEWL (Hirai *et al.*, 1998, 1999; Arai & Hirai, 1999). We can recognize a difference in structural stability between MY and ApoMY with pH variation. In the case of ApoMY the peak height of the Kratky plot at q = ~0.1 Å^{-1} varies slightly with the change of pH, showing that the compactness of the protein structure is influenced more sensitively in comparison with the case of MY (Kataoka *et al.*, 1995). The pH dependence of the radius of gyration R_g is shown in Fig. 3, where R_g is known to be a good index of the molecular size of a protein (Kataoka & Goto, 1996). The transition of R_g occurs around pH 4, which is seen to be more evidently for MY. Above pH ~4 the compactness of the tertiary structure holds mostly for both proteins. We can recognize little difference between the folded structures of ApoMY and MY. The R_g of ApoMY is 21.4 ± 1.0 Å at pH 7, which is slightly larger than that of MY, 18.9 ± 1.5 Å. This suggests that the deletion of heme from MY destabilizes and loosens the tertiary structure, as shown previously (Kirste *et al.*, 1969; Goto *et al.*, 1990; Kataoka *et al.*, 1995).

3.2. Stability intramolecular structure of apomyoglobin depending on pH

Fig. 4(*a*) shows the WAXS curves of 0.005 g ml^{-1} ApoMY at 298 K at different pH values from 3.8 to 9.0. As shown experimentally and theoretically (Hirai *et al.*, 2002, 2004), the scattering curves of proteins in the q ranges of less than ~0.2 Å^{-1}, ~0.25–0.8 Å^{-1} and ~1.1–1.9 Å^{-1} mostly correspond to the different hierarchical levels, namely, to the quaternary and tertiary structures, to the inter-domain correlation and the intra-domain structure and to the secondary structure and the closely packed side chains in the hydrophobic cores, respectively. At pH 3.8 the WAXS curve below q = ~0.25 Å^{-1} slightly differs from those at other pH values, which would reflect a molten globule structure. Above pH 4.5 WAXS curves above q = ~0.25 Å^{-1} agree with each other within experimental errors, indicating that the ApoMY mostly holds native-like intramolecular and secondary structures, in spite of the change of pH from 4.5 to 9.0 under the present experimental conditions. Fig. 4(*b*) shows the comparison of the WAXS curve of ApoMY with that of MY at pH 7, where the protein concentrations were 3.0% *w*/*v*. In Fig. 4(*b*) the WAXS curve of ApoMY in the q range from ~0.25 Å^{-1} to ~0.5 Å^{-1} lacks a hump or a modulation in comparison with the case of MY. As the WAXS curve in this q range mostly corresponds to an interdomain correlation within the protein, the difference between ApoMY and MY clearly shows that the lack of heme loosens a rigid domain packing, alternatively induces an intramolecular fluctuation. On the other hand, the WAXS curves in the q ranges of ~0.5–0.8 Å^{-1} and of ~1.1–1.9 Å^{-1} mostly agree with each other, suggesting that the intradomain structure and the packing geometry and content of the secondary structures within ApoMY resemble those of MY.

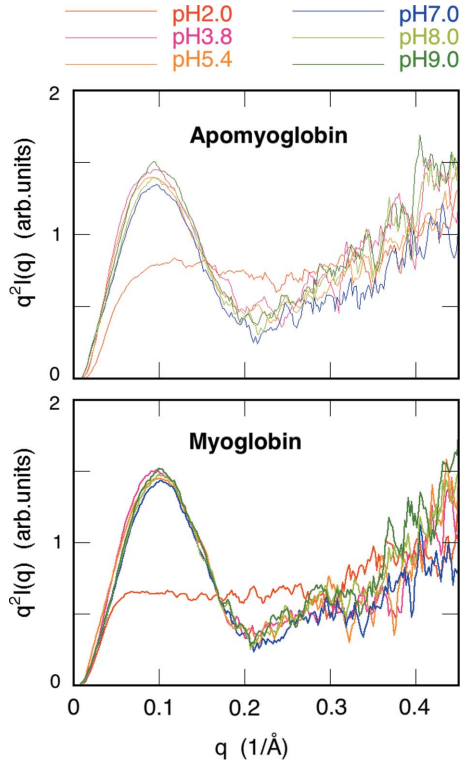

Figure 2
pH dependence of Kratky plots [$q^2I(q)$ *vs* q] of SAXS curves $I(q)$ of ApoMY and MY in Fig. 1.

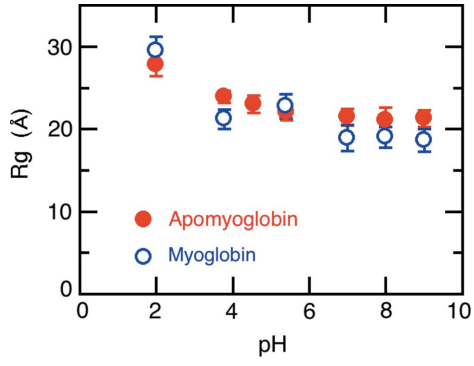

Figure 3
Radii of gyration R_g of ApoMY and MY depending on pH. Data are obtained from Fig. 1 .

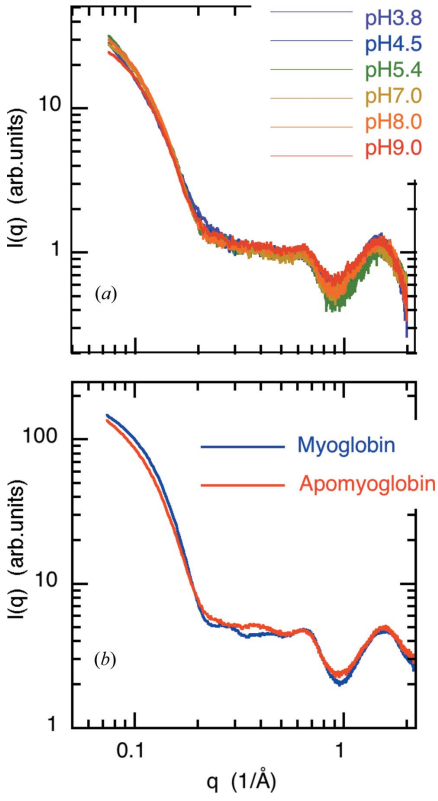

Figure 4
(*a*) WAXS curve of 0.005 g ml^{-1} ApoMY depending on pH; (*b*) comparison of WAXS curves of ApoMY and MY at pH 7.0. The protein concentrations are 0.03 g ml^{-1}.

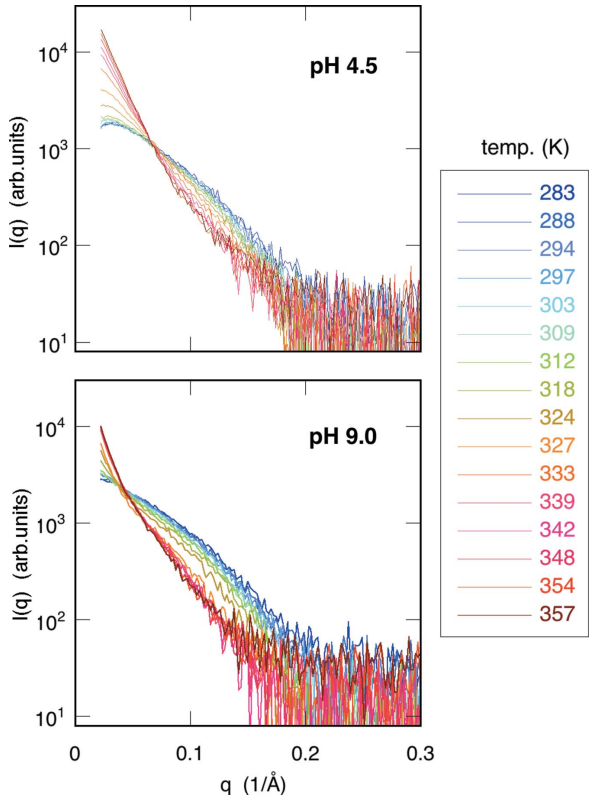

Figure 5
Temperature dependence of the SAXS curves of 0.01 g ml^{-1} ApoMY at pH 4.5 and 9.

3.3. Thermal stability of apomyoglobin in comparison with myoglobin observed by SAXS

Fig. 5 shows the temperature dependence of the SAXS curves of ApoMY of 0.01 g ml^{-1} at pH 4.5 and 9. With elevating temperature, at pH 4.5 the scattering intensity below q = ~0.03 Å^{-1} increases more significantly than that at pH 9, suggesting that in the thermal denaturation process the ApoMY at pH 4.5 takes an expanded structure larger than that at pH 9. The evident change of the SAXS curve starts around 323 K for pH 4.5 and 9.0. As shown in Fig. 6, the temperature dependence of R_g at different pH values supports the above difference between ApoMY and MY. The on-set temperature of the unfolding transition of ApoMY is around 313–318 K and shows little pH dependence above pH 4. In the case of MY at pH 4.5 the on-set temperature locates around 328 K. The difference in the on-set temperatures between ApoMY and MY results from the absence of heme which destabilizes the protein structure, and is in agreement with previous results (Goto *et al.*, 1990; Griko & Privalov, 1994). It is worth noting that the R_g value of ApoMY at pH 9 is smaller than those at pH 4.5 and 5.4, and shows a saturating tendency above 333 K. This suggests that even at the highest temperature ApoMY at pH 9 holds compactness to some extent and does not form large aggregates. A pH of 9 and a temperature of 338 K are the reported conditions of amyloid formation for ApoMY (Fändrich *et al.*, 2001). Therefore, the relatively compact denatured structure or small aggregate of ApoMY at high temperature seems to be a characteristic structure at pH 9, which would be distinct from those at different pH values. The detailed characteristics of the internal structural change of ApoMY at pH 9 depending on temperature can be analyzed by WAXS measurements as shown below.

3.4. Helix-to-cross-β transition and formation of amyloid nuclei of apomyoglobins observed by WAXS

Fig. 7 shows the temperature dependence of WAXS curve of ApoMY at pH 9 and Fig. 8(*a*) shows all WAXS curves at different temperatures superimposed. Based on the WAXS data analyses reported previously (Hirai *et al.*, 2004), we can discuss the structural changes of ApoMY in different hierarchical levels that are the quaternary and tertiary structures (q < ~0.2 Å^{-1}), the inter-domain correlation and the intra-domain structure (q = ~0.25–0.8 Å^{-1}), and the secondary structure and the closely packed side chains in the

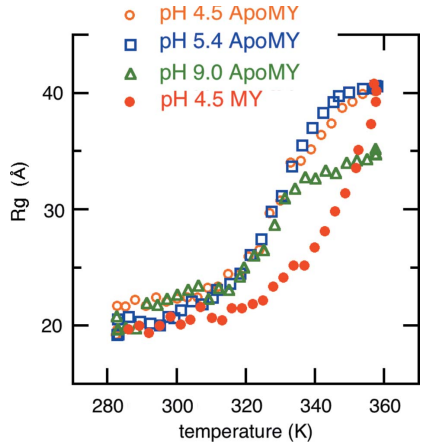

Figure 6
Change of the radius of gyration R_g of 0.01 g ml^{-1} ApoMY at different pH in comparison with that of 0.01 g ml^{-1} MY at pH 4.5. The R_g values were obtained from Fig. 5.

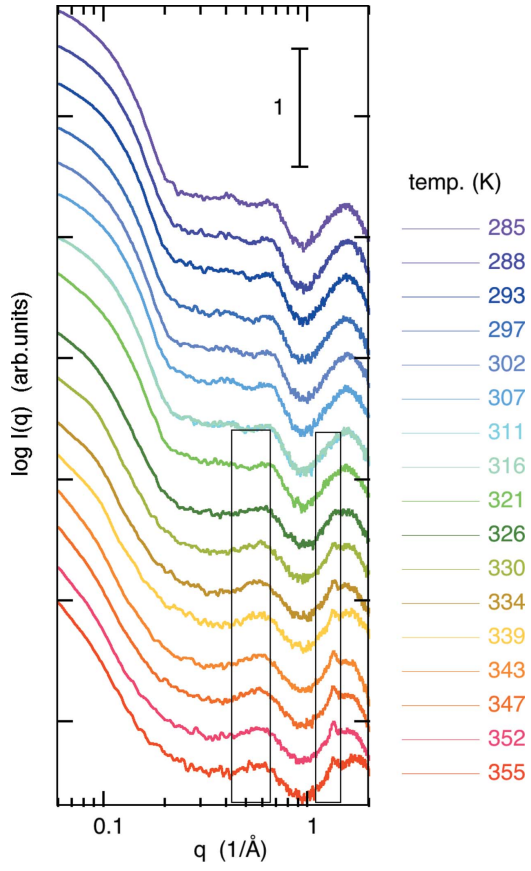

Figure 7
Temperature dependence of the WAXS curve of 0.01 g ml^{-1} ApoMY at pH 9. The open boxes indicate the q-ranges where the typical changes in the WAXS curves are observed in the case of amyloid formation.

hydrophobic cores (q = ~1.1–1.9 Å^{-1}), respectively. In Figs. 7 and 8(a), the slope of the scattering curve below q = 0.15 Å^{-1} changes significantly with elevating temperature from 285 K to 355 K, indicating the change of the tertiary structure of ApoMY that is also shown by the SAXS measurement in Fig. 6. On the other hand, the scattering intensities around the q regions of ~0.55–0.65 Å^{-1} and ~1.2–1.4 Å^{-1} also show evident changes with elevating temperature. In Figs. 7 and 8(a), the peaks around q = ~0.58 Å^{-1} and q = ~1.34 Å^{-1} become to be evident from 326 K. These two peaks are the typical ones for an amyloid formation. The former and later peaks result from the formations of the pleated sheet stacking and the cross-β structure, respectively. The positions of the peaks at q = ~0.58 Å^{-1} and ~1.34 Å^{-1} correspond to the real space distances of ~10.8 Å and ~4.69 Å, respectively. These values agree with those reported previously within experimental errors (Fändrich *et al.*, 2001). In Fig. 8(b) the integrated peak intensities in the q regions of ~0.52–0.64 Å^{-1} and ~1.28–1.4 Å^{-1} are plotted against temperature, where those intensities are normalized by the integrated intensities in the q regions of ~0.25–0.8 Å^{-1} and ~1.1–1.9 Å^{-1}, respectively. Clearly the increase of the intensity starts at ~326 K for both regions. This temperature is slightly higher than the on-set temperature of the tertiary structure transition of ApoMY at pH 9 shown in Fig. 6. The growth of the peak at q = ~1.34 Å^{-1} tends to saturate above ~333 K, whereas the peaks at q = ~0.58 Å^{-1} continue to increase above the on-set temperature. In spite of the appearance of the peak of the cross-β structure, the scattering curve in the q region of ~1.1–1.9 Å^{-1} mostly holds a rounded hump profile. As shown previously (Hirai *et al.*, 2002, 2004), the scattering curve in this region reflects well the secondary structures and the close packed side chains in the hydrophobic cores and, therefore, it is possible to estimate a change occurring in secondary structures. A rounded hump profile in the q region of ~1.1–1.9 Å^{-1} is especially typical for hemoglobin and MY (Hirai *et al.*, 2002) which are classified into all-α proteins according to the Structure Classification Of Proteins database (SCOP; Murzin *et al.*, 1995). Thus, the change of the scattering curve in the q region of ~1.1–1.9 Å^{-1} suggests that the helix-to-sheet structural transition occurs locally within ApoMYs. Figs. 7 and 8(b) show that the cross-β formation and the pleated sheet stacking start concurrently around the same temperature and that the stacking continues progressively after the saturation of the cross-β formation. Noticeably, the cross-β formation and the pleated sheet stacking of ApoMY starts from ~326 K which is a little higher than the on-set temperature of the tertiary structural change in Fig. 6, and ~326 K would mostly agree with the lowest temperature reported for the amyloid formation (Fändrich *et al.*, 2003).

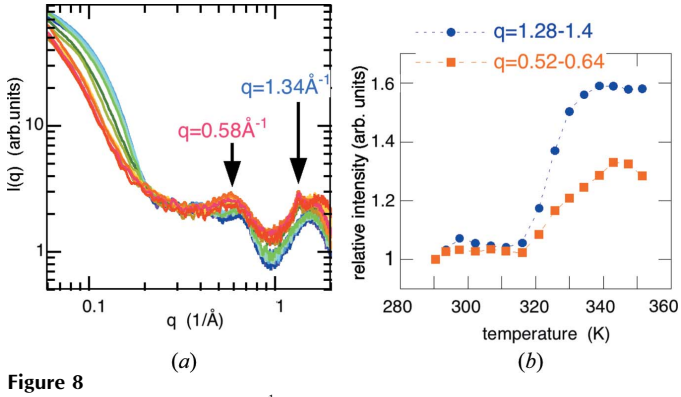

Figure 8
(a), WAXS curves of 0.01 g ml^{-1} ApoMY at pH 9.0, all WAXS curves at different temperatures in Fig. 7 are superimposed. The arrows at q = ~1.34 Å^{-1} and at q = ~0.58 Å^{-1} correspond to the cross-β structure and the pleated sheet stacking in amyloid ApoMY, respectively. (b) Temperature dependence of integrated peak intensities in the q regions of ~0.52–0.64 Å^{-1} and of ~1.28–1.4 Å^{-1}, where those intensities are normalized by the integrated intensities in the q regions of ~0.25–0.8 Å^{-1} and of ~1.1–1.9 Å^{-1}, respectively.

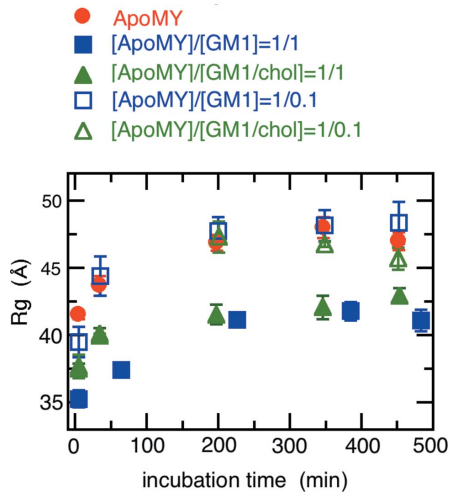

Figure 9
Incubation time dependence of the radii of gyration of ApoMY, ApoMY+G_{M1}, ApoMY+G_{M1}/cholesterol at 328 K at pH 9.0. The molar ratios of [ApoMY]/[G_{M1}] are indicated in the figure. The molar ratio of G_{M1}/cholesterol mixture is 1:1. The incubation started after the addition of lipids.

3.5. Effect of glycosphingolipid G_{M1} on amyloid formation

Under the incubation conditions of 328 K and pH 9, we have monitored the growing process of amyloid nuclei for ~8 h. Fig. 9 shows the time dependence of the radius of gyration after the addition of G_{M1} micelle and $[G_{M1}]$/[cholesterol] = 1/1 mixed vesicle. The $[G_{M1}]$/[cholesterol] = 1/1 mixture corresponds mostly to the raft fraction and forms a small vesicle (Hayakawa & Hirai, 2003). At the high molar ratio of [ApoMY]/$[G_{M1}]$ = 1/1 the growth of the ApoMY aggregate (amyloid ApoMY) is evidently suppressed in both cases of the additions of the micelle and the vesicle. Whereas, at the low molar ratio of [ApoMY]/$[G_{M1}]$ = 1/0.1 the growth of the aggregates is less suppressed, which is mostly same as in the case without the addition of G_{M1}. The present results disagree with the previous report that G_{M1} promotes the growth of amyloid of Aβ proteins (Matsuzaki & Horikiri, 1999). However, it might happen for different types of amyloid-like aggregates such as ApoMY since ApoMY is much larger than Aβ. We need further experiments under different conditions to confirm if ganglioside molecules can induce or accelerate amyloid formation of proteins other than Aβ.

The SAXS and WAXS experiments were carried out under the approval of the Photon Factory Program Advisory Committee of KEK (Proposal #2004G177) and of the JASRI Program Advisory Committee (Proposal #2004A0399 and #2003 A0558).

References

Anfinsen, C. B. (1973). *Science*, **181**, 223–230.
Arai, S. & Hirai, M. (1999). *Biophys. J.* **76**, 2192–2197.
Choo-Smith, L. P., Garzon-Rodriguez, W., Glabe. C. G. & Surewicz, W. K. J. (1997). *Biol. Chem.* **272**, 22987–22990.
Dobson, C. M. (2004). *Methods*, **34**, 4–14.
Dyson, H. J. & Wright, P. E. (2004). *Chem. Rev.* **104**, 3607–36022.
Fändrich, M., Fletcher, M. A. & Dobson, C. M. (2001). *Nature*, **410**, 165–166.
Fändrich, M., Forge, V., Buder, K., Kittler, M., Dobson, C. M. & Diekmann, S. (2003). *Proc. Natl Acad. Sci. USA*, **100**, 15463–15468.
Gekko, K. & Hasegawa, Y. (1986). *Biochemistry*, **25**, 6563–6571.
Goto, Y., Calciano, L. J. & Fink, A. L. (1990). *Proc. Natl Acad. Sci. USA*, **87**, 573–577.
Grateau, G., Kyle, R. A. & Skinner, M. (2004). Editors. *Amyloid and Amyloidosis*. USA: CRC Press.
Griko, Y. V. & Privalov, P. L. (1994). *J. Mol. Biol.* **235**, 1318–1325.
Hakomori, S. (2001). *Trends Glycosci. Glycotechnol.* **13**, 219–230.
Hayakawa, T. & Hirai, M. (2003). *J. Appl. Cryst.* **36**, 489–493.
Hayashi, H., Kimura, N., Yamaguchi, H., Hasegawa, K., Yokoseki. T., Shibata, M., Yamamoto, N., Michikawa, M., Yoshikawa, Y., Terao, K., Matsuzaki, K., Lemere, C. A., Selkoe, D. J., Naiki, H. & Yanagisawa, K. (2004). *J. Neurosci.* **19**, 4894–4902.
Hirai, M., Arai, S. & Iwase, H. (1999). *J. Phys. Chem. B*, **103**, 549–556.
Hirai, M., Arai, S., Iwase, H. & Takizawa, T. (1998). *J. Phys. Chem. B*, **102**, 1308–1313.
Hirai, M., Iwase, H., Hayakawa, T., Koizumi, M. & Takahashi, H. (2003). *Biophys. J.* **85**, 1600–1610.
Hirai, M., Iwase, H., Hayakawa, T., Miura, K. & Inoue, K. (2002). *J. Synchrotron Rad.* **9**, 202–205.
Hirai, M., Koizumi, M., Hayakawa, T., Takahashi, H., Abe, S., Hirai, H., Miura, K. & Inoue, K. (2004). *Biochemistry*, **43**, 9036–9049.
Hirai, M., Koizumi, M., Hirai, H., Hayakawa, T., Yuyama, K., Suzuki, N. & Kasahara, K. (2005). *J. Phys. Condens. Matter*, **17**, s2965–s2977.
Hirai, M. & Takizawa. T. (1998). *Biophys. J.* **74**, 3010–3014.
Hirai, M., Takizawa, T., Yabuki, S., Nakata, Y. & Hayashi, K. (1996). *Biophys. J.* **7**, 1761–1768.
Kataoka, M. & Goto, Y. (1996). *Fold. Des.* **1**, R107–R112.
Kataoka, M., Nishi, I., Fujisawa, T., Ueki, T., Tokunaga, F. & Goto, Y. (1995). *J. Mol. Biol.* **249**, 215–228.
Kirste, R. G. & Oberthür, R. C. (1982). In *Small Angle X-ray Scattering* edited by O. Glatter & O. Kratky, pp. 387–431. London: Academic Press.
Kirste, R. G., Schulz, G. V. & Stuhrmann, H. B. (1969). *Z. Naturforsch. B*, **24**, 1385–1392.
Kratky, O. & Porod, G. (1949). *Recl Trav. Chim. Pays-Bas*, **68**, 1106–1122.
Matsuzaki, K. & Horikiri, C. (1999). *Biochemistry*, **38**, 4137–4142.
Miura, K., Kawamoto, M., Inoue, K., Yamamoto, M., Kumasaka, T., Sugiura, M., Yamano, A. & Moriyama, H. (2000). *SPring-8 User Experiment Report*, **4**, 168.
Murzin, A. G., Brenner, S. E., Hubbard, T. & Chothia, C. (1995). *J. Mol. Biol.* **247**, 536–540.
Oliveberg, M. & Wolynes, P. G. (2006). *Q. Rev. Biophys.* **19**, 1–44.
Pain, R. H. (2000). Editor. *Mechanisms of Protein Folding*. Oxford University Press.